

Large-amplitude isothermal fluctuations and high-density dark-matter clumps

Edward W. Kolb*

*NASA/Fermilab Astrophysics Center,
Fermi National Accelerator Laboratory, Batavia, IL 60510, and
Department of Astronomy and Astrophysics, Enrico Fermi Institute
The University of Chicago, Chicago, IL 60637*

Igor I. Tkachev†

*NASA/Fermilab Astrophysics Center
Fermi National Accelerator Laboratory, Batavia, IL 60510, and
Institute for Nuclear Research of the Academy of Sciences of Russia
Moscow 117312, Russia*

Large-amplitude isothermal fluctuations in the dark matter energy density, parameterized by $\Phi \equiv \delta\rho_{\text{DM}}/\rho_{\text{DM}}$, are studied within the framework of a spherical collapse model. For $\Phi \gtrsim 1$, a fluctuation collapses in the radiation-dominated epoch and produces a dense dark-matter object. The final density of the virialized object is found to be $\rho_F \approx 140 \Phi^3 (\Phi + 1) \rho_{\text{EQ}}$, where ρ_{EQ} is the matter density at equal matter and radiation energy density. This expression is valid for the entire range of possible values of Φ , both for $\Phi \gg 1$ and $\Phi \ll 1$. Some astrophysical consequences of high-density dark-matter clumps are discussed.

PACS number(s): 98.80.Cq, 14.80.Gt, 05.30.Jp, 98.70.-f

*Electronic mail: rocky@fnas01.fnal.gov

†Electronic mail: tkachev@fnas13.fnal.gov

I. INTRODUCTION

In almost all modern cosmological models, galaxies, clusters, and all large-scale structures develop through the gravitational instability of small-amplitude, seed density fluctuations. In most of these models cold dark matter is an important constituent of the total mass density of the Universe. There are two basic types of seed density fluctuations, curvature and isocurvature,¹ and in general, both are expected to be produced in the early Universe. By definition, the total energy density in an isocurvature fluctuation is constant; the fluctuation is in the relative contribution to the total energy density of different components in a multicomponent system. Important examples of this type are the fluctuations induced in the baryons by some dissipative process in a Universe containing both baryons and dark matter, and topological or non-topological field configurations like cosmic strings or textures. While the amplitude of either type of fluctuation on large scales is strongly restricted by microwave background anisotropy constraints, the amplitude of small-scale fluctuations can be large, even non-linear, at the epoch of last scattering. The spectrum of small-scale fluctuations do not necessarily have to reflect the shape of the power spectrum of the primordial fluctuations generated at the inflationary epoch, since the small-scale fluctuations may well be generated later, e.g., during various cosmological phase transitions.

In this paper we are interested in isocurvature fluctuations that enter the horizon before the temperature of equal energy densities of matter and radiation, $T_{\text{EQ}} = 5.5 \Omega_0 h^2 \text{ eV}$ [2]. We will consider scales much smaller than the horizon, so the radiation energy density should be homogeneous.

It is well known [3] that the growth of small-amplitude isothermal fluctuations is

¹The division of fluctuations into curvature and isocurvature is strictly true only outside the Hubble radius [1].

suppressed by the cosmological expansion, and the fluctuations do not grow until after the equality epoch. However, this is true only in linear theory. The self gravity of large-amplitude, non-linear fluctuations may become important before T_{EQ} , and consequently they collapse earlier. Therefore they are capable of producing very dense objects after they separate out from the general expansion and virialize.

We refer to these isothermal fluctuations as “clumps.”² Let us specify the density of a dark-matter clump as

$$\delta\rho_{\text{DM}}/\rho_{\text{DM}} = \Phi, \tag{1.1}$$

where Φ is not necessarily small. For example, “typical” axion miniclusters [4] will have $\Phi \sim 1$. In Ref. [6] it was found that accounting for non-linear effects in the evolution of axions at the crucial epoch when the axion mass switches on can lead to considerably larger density in many miniclusters, with Φ in the range 1 to 10^4 . Dark-matter clumps seeded by wakes induced by cosmic strings or by textures also will have $\Phi \sim 1$ [5]. *Seeded clumps are particularly interesting in the case of WIMP dark matter*

It was pointed out in Ref. [6] that the final virialized density in a clump has to scale as $\rho_F \sim \Phi^4 \rho_{\text{EQ}}$. Because of the dependence upon the fourth power of Φ , even a small increase in Φ is very important. For the same reason, the final density can be sensitive to the details of the evolution of the clump in the radiation-dominated era. To our knowledge, a detailed study of the non-linear evolution of large-amplitude isothermal fluctuations has never been performed. However, it is very important in various phenomenological implications including both direct and non-direct dark matter searches. In this paper we consider this problem.

The clumpiness of the dark matter has important implications for attempts to detect dark matter. Clearly the signal in direct detection experiments for dark matter is pro-

²Since the clumps may be very dense compared to the background, we do not refer to them as “perturbations.”

portional to the dark matter density. For the rare direct encounter with a clump, there could be a huge amplification of the signal. However, if the clumpiness is too high, the flux of unclumped dark matter will be too small for a reasonable detection rate. The rate of WIMP annihilation contributing to the γ -ray background [7,8] is proportional to the density as well. In the case of clumped dark matter, there will be stronger constraints on dark matter from indirect searches. In very dense axion clumps, Bose star formation becomes possible [9] (clumps with $\Phi \sim 30$ already satisfy the critical condition for this [6]), which in turn can lead to the formation of radio sources [10]. Another possible manifestation of high density clumps is the phenomenon of microlensing.

To study the structure and evolution of high density clumps, a full 3-dimensional numerical simulation is needed. However, for an isolated clump some relevant physical information can be extracted from a 1-dimensional spherical model. The spherical model proved useful in studies of the gravitational non-linear evolution in the epoch of matter domination when it is possible to find exact analytic solutions [11]. In the present paper we generalize this model to include radiation. Although there are no analytic solutions, the result turns out to be very simple: The final density in a virialized clump is $\rho_F \approx 140 \Phi^3 (\Phi + 1) \rho_{\text{EQ}}$ in the whole range of possible values of Φ , both for $\Phi \gg 1$ and for $\Phi \ll 1$.

II. A SPHERICAL MODEL

Let us consider a spherical region of radius r containing an overdensity of pressureless matter in an expanding Universe. In a spatially flat Universe, every overdense region eventually reaches some maximum size and re-collapses. The total mass of matter in the region inside r , M_{TOT} , is an integral of the motion so long as the region expands. Since we

will consider scales much smaller than the Hubble radius, we can consider the radiation to be homogeneous, with its time evolution determined by the general expansion of the Universe, and not by the local conditions.

The equation of motion for the radius of the region is

$$\ddot{r} = -\frac{8\pi G}{3}\rho_R - \frac{GM_{\text{TOT}}}{r^2}. \quad (2.1)$$

It is convenient to change to the conformal time coordinate, $d\eta = dt/a(t)$, and then to rewrite this equation of motion in the comoving reference frame, $r = a(\eta)R_\xi(\eta)\xi$, where ξ is the comoving label of a given shell and $R_\xi(\eta)$ measures the deviation of the shell motion from the uniform Hubble flow of the background Friedmann Universe. In what follows we shall omit the subscript ξ on $R(\eta)$, but it should be understood that there is a separate evolution for each shell.

We shall assume that the scale factor $a(\eta)$ satisfies the Einstein equations for an $\Omega_0 = 1$ Universe filled with radiation and pressureless matter:

$$a'^2 = \frac{8\pi G}{3}(\rho_M + \rho_R)a^4; \quad a'' = \frac{4\pi G}{3}\rho_M a^3, \quad (2.2)$$

where prime denotes $d/d\eta$. We parametrize the radiation and matter energy densities as, $\rho_R = \rho_{\text{EQ}}(a_{\text{EQ}}/a)^4$ and $\rho_M = \rho_{\text{EQ}}(a_{\text{EQ}}/a)^3$. The solution to the background equations, Eqs. (2.2), is

$$a(\eta) = a_{\text{EQ}}[2(\eta/\eta_*) + (\eta/\eta_*)^2], \quad (2.3)$$

where $\eta_*^{-2} = 2\pi G\rho_{\text{EQ}}a_{\text{EQ}}^2/3$.

The equation of motion [Eq. (2.1)] in terms of conformal time is

$$aR'' + a'R' + \left(\frac{GM_{\text{TOT}}}{\xi^3 R^2} - \frac{4\pi G}{3}a^3\rho_M R \right) = 0. \quad (2.4)$$

The radiation energy density does not enter this equation explicitly, but its effect is encoded in the evolution of the scale factor. We also parametrize the total mass of

matter inside the shell in terms of the excess over the homogeneous background, denoted as $\Phi(\xi) \equiv \delta\rho_M/\rho_M$. The total mass within the region is

$$M_{\text{TOT}} \equiv \frac{4\pi}{3}\rho_{\text{EQ}}a_{\text{EQ}}^3[1 + \Phi(\xi)]\xi^3. \quad (2.5)$$

Changing from η to $x \equiv a/a_{\text{EQ}}$ as the independent variable, we finally obtain

$$x(1+x)\frac{d^2R}{dx^2} + \left(1 + \frac{3}{2}x\right)\frac{dR}{dx} + \frac{1}{2}\left(\frac{1+\Phi}{R^2} - R\right) = 0. \quad (2.6)$$

This equation reduces to the Meszaros equation [3] in the limit of small deviation of the shell motion from the general cosmological expansion, $R \equiv 1 - \delta$ and $\delta \ll 1$, if we assume no excess in total mass of the matter, i.e., $\Phi = 0$,

$$x(1+x)\frac{d^2\delta}{dx^2} + \left(1 + \frac{3}{2}x\right)\frac{d\delta}{dx} - \frac{3}{2}\delta = 0. \quad (2.7)$$

The latter is hypergeometric equation, and its growing mode is $\delta = \delta_0(1+3x/2)$, implying the well known result that the growth of small fluctuations is significant only after the Universe becomes matter dominated.

We have solved Eq. (2.6) numerically, assuming $R(x_0) = 1$ at some early time, $x_0 \ll 1$. Note that at small x , the second derivative in Eq. (2.6) can be neglected, and the solution with initial conditions fixed at $x_0 = 0$ is $R = (1 - 3\Phi x/2)^{1/3} \simeq 1 - \Phi x/2$, where the expansion is justified since the solution is valid only at small x . Actually, this is the separatrix, i.e., independently of the initial value of R' , all solutions tend to it (provided $x_0 \ll 1$). The results of numerical integration of Eq. (2.6) proved to be insensitive to $R'(x_0)$ already at $x_0\Phi < 10^{-3}$. For several different values of Φ they are shown in Fig. 1.

It is possible to find an analytic approximation to $R(x)$ as a power series in x to any given order. To third order it is

$$R = 1 - \frac{\Phi x}{2} - \frac{\Phi^2 x^2}{8} - \frac{(8\Phi^3 - \Phi^2)x^3}{144}. \quad (2.8)$$

The first three terms in this decomposition provide a good practical fit to the solution. This fit is shown in Fig. 1 by the dotted line. The last term in Eq. (2.8) shows that the solution is not simply a function of the product Φx .

Our main goal is to find the parameters of the fluctuation, i.e., its radius and density, at the moment when the fluctuation turns around. For later times the assumption of spherical symmetry breaks down; however, we can assume that the radius of a virialized gravitationally bound object will be one-half of the turnaround radius, and the density inside the object will be eight times larger than the density at turnaround [11]. The turnaround time, defined by $\dot{r} = 0$, in coordinates of Eq. (2.6) is the solution to the equation $R + x dR/dx = 0$. Up to order $\mathcal{O}(x^2)$ the function R only depends upon the product Φx , so to this order in x the scale factor at turnaround will be given by $x_{\text{TA}} = \text{const}/\Phi$ and to the same order in x , $R_{\text{TA}} = \text{const}$. The matter density of a fluctuation at turnaround is $\rho_{\text{TA}} = (1/4\pi r^2)dM/dr$, with $r = R_{\text{TA}}x_{\text{TA}}\xi$, so it is appropriate to represent the parameters at turnaround as

$$x_{\text{TA}} = C_x/\Phi; \quad \rho_{\text{TA}} = C_\rho \rho_{\text{EQ}} \frac{\Phi^3}{3\xi^2} \frac{d}{d\xi} (1 + \Phi)\xi^3. \quad (2.9)$$

We expect only a weak dependence of C_x and C_ρ upon Φ , since higher order corrections are small. Results of a numerical integration for C_x and C_ρ are shown in Fig. 2 and Fig. 3 respectively. These figures demonstrate that for practical applications we can consider C_x and C_ρ to be constants in entire range of possible values of Φ , both $\Phi \gg 1$ and $\Phi \ll 1$.

Let us compare our results to predictions of a standard spherical model, which is valid for the matter-dominated epoch, i.e., at small Φ . The spherical model predicts $\rho_{\text{TA}}/\rho_{\text{B}} = 9\pi^2/16$ for the density contrast at turnaround, where ρ_{B} is the background density [11]. Using Fig. 2 we can extract the corresponding values of ρ_{B} and then calculate the standard spherical model prediction for C_ρ . This is presented in Fig. 3 by the dashed line. Both dashed and solid lines coincide in the limit of small Φ , as they must.

III. APPLICATIONS

With the function $\Phi(\xi)$ in the general form we have assumed, the effective radius after virialization for each shell of a given label ξ will be half the turnaround radius of the shell.³ Using Eq. (2.9) we obtain for the final density profile in a virialized object

$$\rho_F \approx 140\rho_{\text{EQ}} \frac{\Phi^3}{3\xi^2} \frac{d}{d\xi} (1 + \Phi)\xi^3, \quad (3.1)$$

where we have set $C_\rho \sim 17$. For the core density, this formula gives $\rho_F \approx 140 \Phi_0^3 (\Phi_0 + 1)\rho_{\text{EQ}}$, where $\Phi_0 = \Phi(0)$. The numerical value of the density at equality is $\rho_{\text{EQ}} \approx 3 \times 10^{-16} (\Omega h^2)^4 \text{g cm}^{-3}$. Now let us turn to a few specific examples.

A. Axion miniclusters

Fluctuations in the density of axions can be very high, possibly spanning the range $1 \lesssim \Phi \lesssim 10^4$ [6,12]. Even with Φ as small as 1, the density in miniclusters which form out of these fluctuations can be as much as 10^{10} times larger than the local galactic halo density [4]. Using Eq. (3.1), we obtain $\rho_F \sim 9 \times 10^{-14} \Omega^4 h^8 \text{g cm}^{-3}$ for $\Phi = 1$. With $\Phi \gg 1$ this result must be multiplied by $\Phi^4/2$.

The typical mass of an axion minicluster corresponds to the total mass in axions within the horizon at $T \sim 1 \text{ GeV}$ when the inverse axion mass is equal to the Hubble length: $M_{\text{MC}} \sim 10^{-9} M_\odot$. The present probability of a direct encounter with a minicluster is small, the encounter rate is 1 per 30 million years with $\Phi = 1$. Although the signal in an axion detector [13] from a close encounter would be enormous, it might be a long wait with a weak signal between encounters if a major fraction of the axions are part of miniclusters.

There should be some miniclusters with Φ in the range $10^{-3} \lesssim \Phi \lesssim 1$. These collapse

³Strictly speaking this is not always true, but for the practical applications we will consider below the approximation should be reasonable.

during the matter-dominated epoch and have a larger radii than those with $\Phi \gtrsim 1$ which collapsed in the radiation-dominated epoch, so the probability of an encounter with a clump with $\Phi \ll 1$ can be larger. From the point of view of direct searches, even miniclusters with density contrast of order two times the average with respect to the galactic halo density are important. Such miniclusters form just prior to the moment of galaxy formation and started with $\Phi \sim 10^{-3}$. For $\Phi < 1$ the expected time between encounters is given in terms of the number density of clumps, n , the geometric cross section of the clump $\sigma \sim R_{\text{CLUMP}}^2$, and the virial velocity v as

$$\tau = \frac{1}{n\sigma v} \simeq \frac{1}{\Phi} \frac{\rho_F}{\rho_H} \frac{R_{\text{CLUMP}}}{v}, \quad (3.2)$$

where ρ_H is the halo density, and R_{CLUMP}/v is the time the Earth spends inside the minicluster. The factor of Φ^{-1} appears because the number density of miniclusters with $\Phi \ll 1$ is suppressed in our model. A minicluster with $\Phi \ll 1$ would require the initial misalignment angle θ (which is uniformly distributed in the range 0 to 2π) to be finely tuned to the mean misalignment angle to an accuracy $\delta\theta/\theta \simeq \Phi/2$. Using Eq. (2.9), we finally obtain

$$\tau = \Phi\tau_{\Phi=1} = \Phi \cdot 3 \times 10^7 \text{ yr}. \quad (3.3)$$

Note that the miniclusters discussed so far appear if the axion field is uncorrelated on scales larger than the Hubble radius at $T \sim 1$ GeV. However miniclusters with $\Phi \ll 1$ can appear from primordial density fluctuations generated by inflation without the suppression factor of Φ^{-1} . If this is the case, then $\tau \simeq \Phi^2 \cdot 3 \times 10^7$ yr. Since Φ would be small, this would give a reasonable encounter rate, and the question of formation and survival of small-scale clumps within the galaxy is worth further study.

Another astrophysical outcome of very dense axion clumps can be the possibility of ‘‘Bose star’’ formation in axion miniclusters. The Bose-Einstein relaxation time in the

minicluster due to axion self-interaction is smaller than the present age of the Universe with $\Phi \gtrsim 30$ [6,9].

B. Accretion by a point mass

The density profile in the halo accreted by a previously formed clump can be calculated in the approximation of secondary infall onto an excess point mass of mass m . In this case $\Phi(\xi) = m/M$, where $M = 4\pi\rho_{\text{EQ}}a_{\text{EQ}}^3\xi^3$ is the mass of the background dark matter within the shell with the label ξ . Substituting this into Eq. (3.1) we find

$$\rho_F \approx 140\rho_{\text{EQ}}(m/M)^3. \quad (3.4)$$

This can be translated into ρ_F as a function of r since M has to be understood as the mass of dark matter residing within r . The result is $\rho_F \propto r^{-9/4}$, the same power law one usually obtains for secondary infall in the matter-dominated era [14]. However, Eq. (3.4) is valid regardless of the time when collapse actually occurs.

C. Cosmic strings

We can apply Eq. (3.4) for clumps of dark matter seeded by loops of cosmic strings so long as the peculiar velocity of a loop is sufficiently small. Since the string loop is not a point object, this formula breaks down in the region of small M . Namely, when the given shell turns around at $x_{\text{TA}} \approx 0.7M/m$, the loop size l_S has to be smaller than the physical radius of the shell, $r_{\text{TA}} = x_{\text{TA}}R_{\text{TA}}\xi a_{\text{EQ}}$, for Eq. (3.4) to be valid. This gives the restriction $M \gtrsim 3m^{3/2}\mu^{-3/4}\rho_{\text{EQ}}^{1/4} \equiv M_C$, where $m = \mu l_S$. We can consider M_C as the mass of the core region. The corresponding maximum density which can be achieved in the core is $\rho_C \sim 15\sqrt{\mu^3\rho_{\text{EQ}}}/M_C$. This value of the core density could be many orders of magnitude larger than the density at equality. However, as we see from Eq. (3.4), ρ_F is much greater than ρ_{EQ} only in the case when the mass of the string loop is larger than the mass of the accreted dark matter. Consequently, with

gradual loop decay due to emission of gravitational radiation, the dark matter clump will adiabatically expand and diminish in density. This process of clump expansion will continue until $m \lesssim M$. Since in the gravitational field the product rm is an adiabatic invariant for each dark matter particle, where r is the effective radius of the orbit, we conclude that in any clump for which $M < m$ initially, the present density will have the same order of magnitude, $\rho \sim 10^2 \rho_{\text{EQ}}$. Dark-matter clumps seeded by wakes induced by long segments of moving cosmic strings or by textures also will have $\Phi \sim 1$ (see [5]), and correspondingly the same virialized density, $\rho \sim 10^2 \rho_{\text{EQ}}$. While this density is sufficiently high to be significant in applications like annihilation of dark matter particles, it is too small to cause microlensing, as we show below.

Cold dark matter accretion onto string loops both in the matter and radiation dominated era was also considered in Ref. [15], however, only in the linearized limit of Eq. (2.6), i.e., Eq. (2.7).

D. WIMP annihilation

In the case where the dark-matter particle species is a stable weakly interacting massive particle (WIMP) such as a very massive neutrino or a supersymmetric particle (photino, higgsino, or scalar neutrino), the WIMPs can annihilate, contributing to the γ -ray flux. This places severe constraints on the dark-matter density near the center of the galaxy [7,8]. Clumped dark-matter annihilation is even more efficient, and places a very strong limit on the clumpiness as a function of the WIMP properties [5].

For the γ -ray flux on Earth from WIMP annihilation in the clump, we can write

$$I_\gamma \approx \frac{\langle \sigma v \rangle \rho M}{4\pi r_\odot^2 m_X^2}, \quad (3.5)$$

where r_\odot is the distance from the Earth to the clump ($r_\odot \approx 8.5$ kpc is the distance to the center of the Galaxy), m_X is the particle mass, and M is the mass of the clump. Since the particles are non-relativistic, both in the clumps and at the epoch of cosmological

freeze-out of the WIMPs, the thermal average of the cross-section in the Eq. (3.5) is directly related to the cosmological abundance [16]:

$$\langle\sigma v\rangle\approx\frac{4\times 10^{-27}}{\Omega_X h^2}\text{cm}^3\text{sec}^{-1}.\tag{3.6}$$

If we consider a large region of (possibly) clumpy dark matter, like the galactic core or spheroid, we must sum up the fluxes from each individual clump. As a result, instead of M in Eq. (3.5) we have to substitute ξM_{tot} , where ξ is the mass fraction of all clumps to the total mass M_{tot} in the region. For example, using $\rho\sim 10^2\rho_{\text{EQ}}$ we obtain for the central spheroid ($M_{\text{tot}}\approx 10^8M_\odot$)

$$I_\gamma\approx\xi\Omega_X^3h^6m_{20}^{-2}\text{cm}^{-2}\text{sec}^{-1},\tag{3.7}$$

where $m_{20}\equiv m_X/20$ GeV. This has to be compared to the observed upper limit to the γ -ray flux in the direction of the Galactic center [7], $I_\gamma\approx 4\times 10^{-7}\text{cm}^{-2}\text{sec}^{-1}$.

E. Gravitational microlensing

Two conditions must be satisfied for the clump to cause gravitational microlensing [17]. First, the mass of the clump has to be in a range near $0.1M_\odot$. Second, the physical radius of the clump has to be smaller than the Einstein ring radius, $R_E=2\sqrt{GMd}$ where d is the effective distance to the lens (typically $d\sim 20$ kpc). The second condition restricts the density of the minicluster to be $\rho\gtrsim 10^7\rho_{\text{EQ}}/\sqrt{M_{-1}}$, where $M_{-1}\equiv M/0.1M_\odot$. If the lensing object is a clump of non-interacting cold dark matter, it has to be formed from a density fluctuation with $\Phi\gtrsim 20$.

Dark matter clumps seeded by string loops or textures, which were considered in Ref. [5], are in the appropriate mass range; however, they have $\Phi\sim 1$. Axion miniclusters can have $\Phi\gtrsim 20$; however, they are too light. While it is possible to invent models where both conditions are met for some of the clumps (one example could be an axion model with an extremely small, but non-zero, value for the u -quark mass), it is hardly likely

that a substantial amount of the dark matter has evolved into clumps capable of lensing. On the other hand, anticipating significant numbers of microlensing events (for the first positive reports see Ref. [18]) in the future, it is not excluded that some of them could be caused by the clumps in such classes of models (especially if collisional relaxation is significant). The corresponding light curve will be different from the MACHO event since clumps are extended objects.

When our paper was almost completed we became aware of the paper Ref. [19] where Eq. (2.6) was studied in details; however, again for the case which corresponds to $\Phi \ll 1$.

It is a pleasure to thank S. Colombi, A. Stebbins and R. Caldwell for useful discussions. This work was supported in part by the DOE and NASA grant NAGW-2381 at Fermilab.

-
- [1] W. H. Press and E. T. Vishniac, *Ap. J.* **239**, 1 (1980).
 - [2] E. W. Kolb and M. S. Turner, *The Early Universe*, (Addison-Wesley, Redwood City, Ca., 1990).
 - [3] P. Meszaros, *Astron. Astrophys.* **37**, 225 (1974).
 - [4] C. J. Hogan and M. J. Rees, *Phys. Lett.* **B205**, 228 (1988).
 - [5] J. Silk and A. Stebbins, *Astrophys. J.* **411**, 439 (1993).
 - [6] E. Kolb and I. I. Tkachev, *Phys. Rev. Lett.* **71**, 3051 (1993).
 - [7] J. Silk and H. Bloemen, *Astrophys. J. Lett.* **313**, L47 (1987).
 - [8] J. R. Ipser and P. Sikivie, *Phys. Rev. D* **35**, 3695 (1987).

- [9] I. I. Tkachev, Phys. Lett. **B261**, 289 (1991).
- [10] I. I. Tkachev, Sov. Astron. Lett. **12**, 305 (1986); I. I. Tkachev, Phys. Lett. **B191**, 41 (1987).
- [11] P. J. E. Peebles, *The Large-Scale Structure of the Universe* (Princeton Univ. Press, 1980).
- [12] E. Kolb and I. I. Tkachev, *Non-linear axion dynamics and formation of cosmological pseudo-solitons*, preprint FERMILAB-PUB-93/355-A (unpublished).
- [13] P. Sikivie, Phys. Rev. Lett. **51**, 1415 (1983).
- [14] J. E. Gunn, Astrophys. J. **218** (1977) 592.
- [15] A. Stebbins, Astrophys. J. Lett. **303**, L21 (1986).
- [16] B. Lee and S. Weinberg, Phys. Rev. Lett. **39**, 165 (1977).
- [17] B. Paczynski, Astrophys. J. **304**, 1 (1986); K. Griest, Astrophys. J. **366**, 412 (1991).
- [18] E. Aubourg et al. (EROS Collaboration), *Nature* (1993); C. Alcock et al. (MACHO Collaboration), *Nature* (1993).
- [19] T. Padmanaban and K. Subramanian, Astrophys. J. **417**, 3 (1993).

FIGURE CAPTIONS:

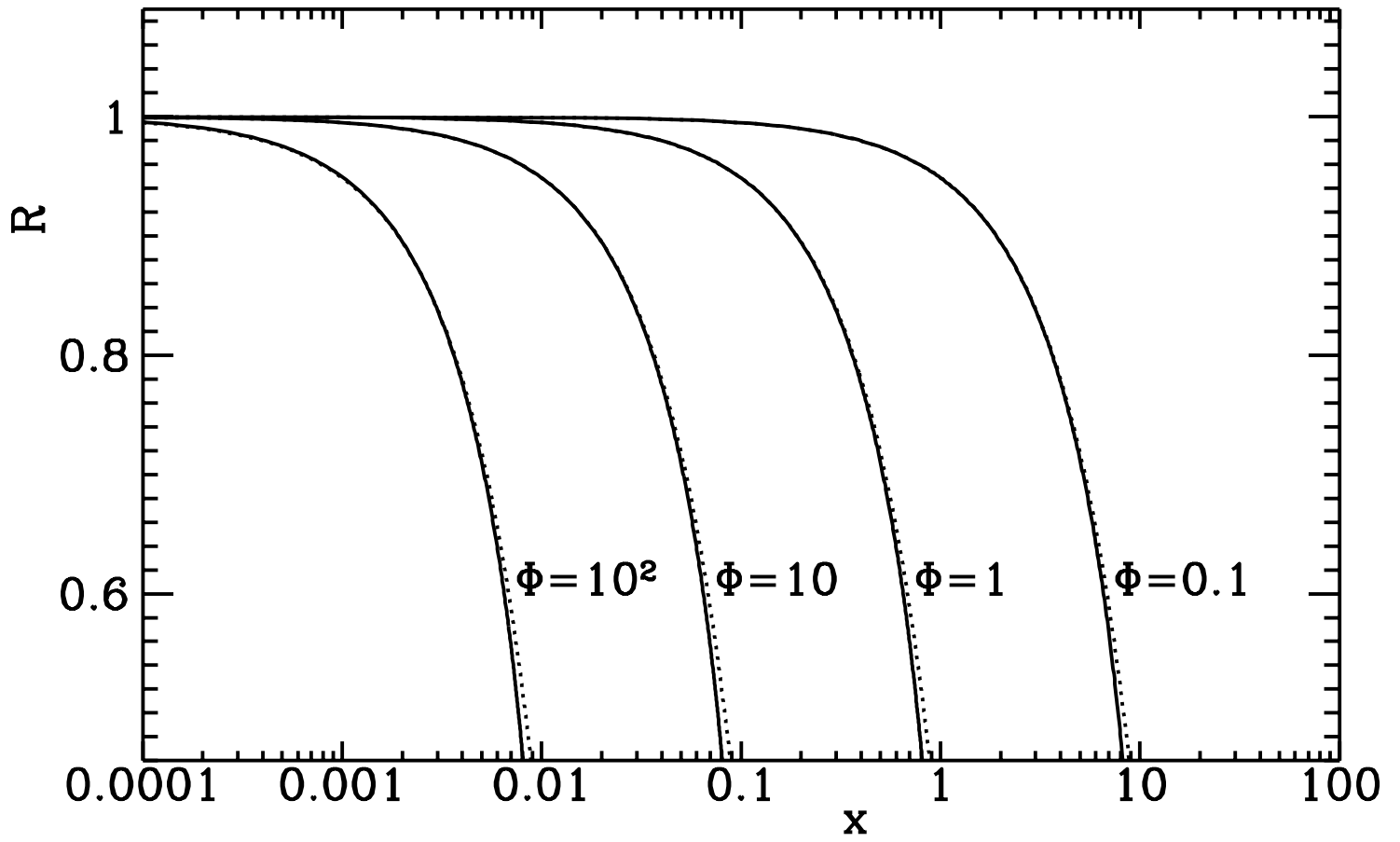
Fig. 1: Numerical solutions to Eq. (2.6) for several different values of Φ . The second-order fit is shown by the dotted line.

Fig. 2: The coefficient C_x in Eq. (2.9) as a function of Φ .

Fig. 3: The coefficient C_ρ in Eq. (2.9) as a function of Φ . The dashed line is the prediction of the standard spherical model (matter without radiation).

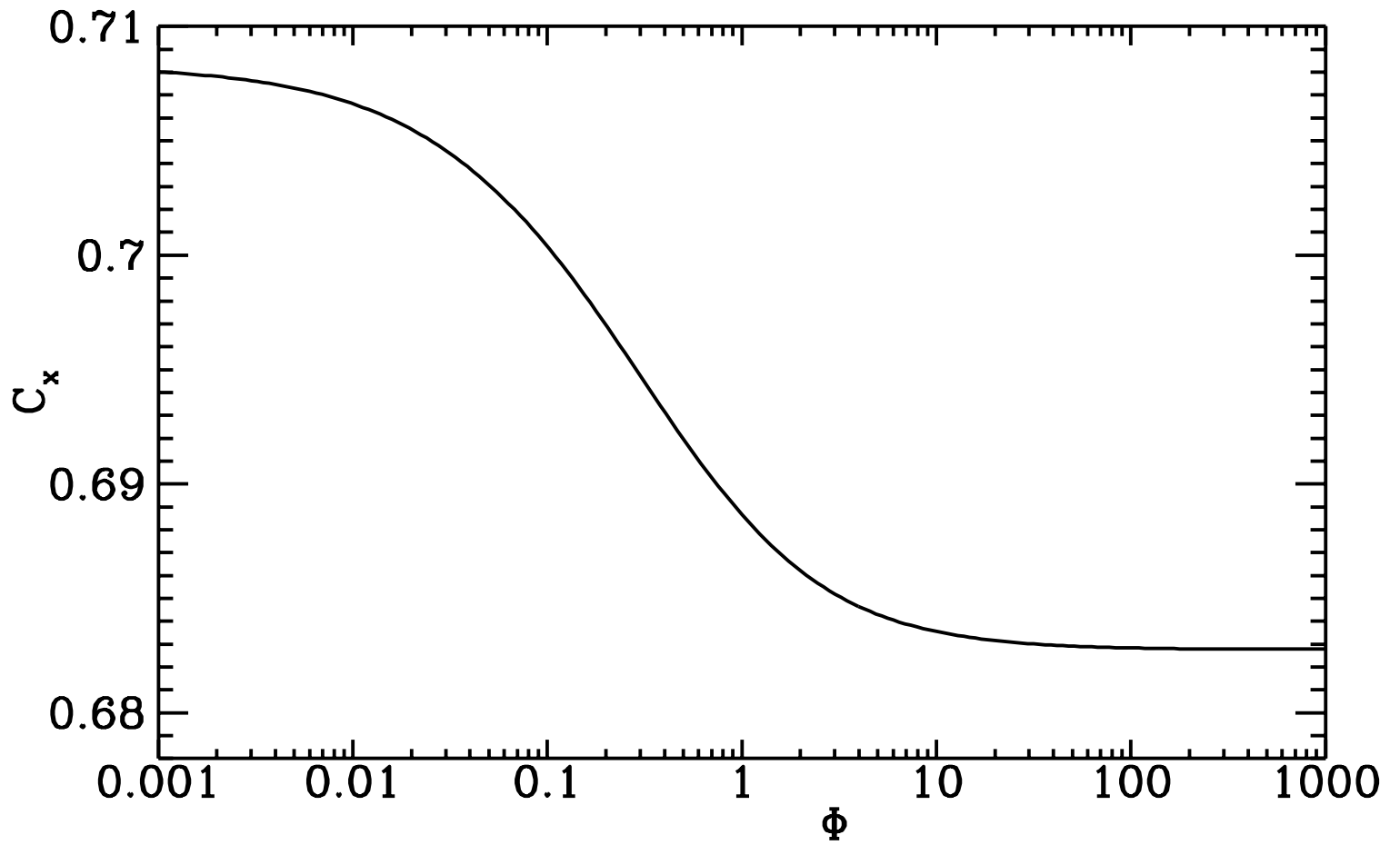
This figure "fig1-1.png" is available in "png" format from:

<http://arxiv.org/ps/astro-ph/9403011v1>



This figure "fig1-2.png" is available in "png" format from:

<http://arxiv.org/ps/astro-ph/9403011v1>



This figure "fig1-3.png" is available in "png" format from:

<http://arxiv.org/ps/astro-ph/9403011v1>

